Influence of carbonation on the microstructure and the gas diffusivity of hardened cement pastes

Mouna Boumaaza, Philippe Turcry, Bruno Huet, Abdelkarim Aït-Mokhtar

Influence of carbonation on the microstructure and the gas diffusivity of hardened cement pastes

Mouna Boumaaza*[1,2,3], Philippe Turcry[2] , Bruno Huet[1], Abdelkarim Aït Mokhtar[2]

[1]*LafargeHolcim research center, 95 rue du Montmurier, 38070 Saint Quentin Fallavier, France*

[2]*Universite de La Rochelle - CNRS, LaSIE UMR 7356 - Laboratoire des Sciences de l'Ingénieur pour l'Environnement, 17000 La Rochelle, France*

[3]*Technische Universität München, cbm Centrum Baustoffe und Materialprüfung Baumbachstraße 7, 81245 München, Deutschland*

ABSTRACT

The influence of carbonation on the oxygen-effective diffusion coefficient ($D_{e,O2}$) of hardened cement pastes (HCP) is investigated in the scope of durability. Experiments are carried out on HCP made with different binders (Portland cement, fly ash, slag, metakaolin binders) and water-to-binder ratios at three relative humidity levels. At a given RH, the change in $D_{e,O2}$ due to carbonation depends on the mix composition. However, in most of cases, $D_{e,O2}$ increases after carbonation, despite the porosity clogging. This is explained by both the decrease in the water saturation degree, especially at high RH, and the change in the pore size distribution. A good correlation is found between the mean pore diameter and gas diffusivity before and after carbonation at low water saturation degree ($R^2 > 0.84$ on a log-log scale). $D_{e,O2}$ is significantly less dependent on the water saturation degree after carbonation.

Key words: Durability; effective diffusion coefficient; carbonation; water retention capacity; pore size distribution.

1. INTRODUCTION

Carbonation is recognized as a significant cause of corrosion in concrete reinforcement [1][2].This physicochemical process causes diverse chemo-mechanical changes in the cement paste, especially changes in the microstructure and chemistry of the cementitious matrix [3][4].

The first mechanism controlling concrete carbonation is the gaseous CO_2 diffusion process by which CO_2 moves through the gas-filled pores. This phenomena is governed by an effective-

diffusion coefficient, which is a durability indicator of concrete, a quality parameter indicating the level of gas tightness of cementitious materials, and a relevant input parameter for service life prediction models of concrete in a real environment [5][6][7]. Previous works [8][9] show that transport properties of cementitious materials are highly dependent on the degree of water saturation. Hence, the determination of transport properties at various hydric states is of high importance. On the other hand, carbonation causes numerous changes in the cement paste microstructure [4][10]. It should be noted that, in the literature, experimental data on the effect of carbonation on gas diffusivity are lacking compared to investigations on other transport phenomena such as chloride diffusion and water transfer [11][12][13]. The microstructure of the hardened cement paste (HCP) determines the transport properties of concrete to a high extent, since HCP is the component that contributes for the greatest part of the concrete porosity [14][15]. Therefore, in the present work, diffusion tests are carried out on HCP samples, employing an experimental setup from our previous works [9]. The latter uses atmospheric oxygen as the diffusing gas and allows for the determination of oxygen diffusivity under different hygrometric conditions. Admittedly, major differences exist between O_2 and CO_2 gases: their solubility in fluids, their molecular size, etc. Nevertheless, it is possible to obtain a good prediction of CO_2 diffusivity by means of values of O_2 diffusivity [16][17]. Plus, the CO_2-effective diffusion coefficient of partially water saturated cementitious materials cannot be measured using gaseous CO_2 since it chemically reacts with the calcium-bearing phases of the materials and changes their microstructure.

The second mechanism controlling the carbonation progress of concrete is the CO_2-binding capacity of its hardened cement paste. This property is directly related to the amount of the calcium-bearing phases that could dissolve and react to result in the formation of calcite. The amount of carbonatable compounds influences the rate of carbonation: a higher amount of carbonatable compounds hinders the carbonation depth progress [5]. Note that the amount of bound CO_2 varies with the different humidity levels in each exposure site: the pastes exposed to the higher humidity (unsheltered from rain) are those fixing a higher amount of CO_2 [18].

The partial replacement of cement with alternative powders entails a considerable environmental impact. However, the use of these additions, also called Supplementary Cementitious Materials (SCMs) should not adversely affect the behavior of the material. SCMs can

be classified into pozzolanic, hydraulic or inert substances. There are great differences in the respective contribution of each SCM's type to the hydration reaction of the cement and, consequently, to the HCP microstructure. Therefore, it is important for the carbonation resistance of cementitious materials to know what role an optional additive plays in the microstructure of the material.

In the present work, the oxygen-effective diffusion coefficient of six different HCPs blended with fly ash, slag, limestone and metakaolin additions is determined after 90 days hydration in the non-carbonated state and after carbonation under 1% CO_2 concentration by volume.

The influence of the degree of water saturation is assessed at both states after a preconditioning at three relative humidity levels: 55%, 95% and 33%. The microstructural changes, phase assemblage and CO_2-binding capacity of the tested HCPs are investigated using water porosity, mercury intrusion porosimetry (MIP), and XRD and TGA techniques, respectively. The carbonation resistance is deduced from this work's results using a deterministic model from the literature. The carbonation performance of the six HCPs is compared to experimental results after exposing the HCPs to carbonation in a room regulated at 50%RH.

2. MATERIALS AND METHODS

2.1 Cement pastes mixtures

With the aim of testing the most widely used binders, six types of cement pastes, including blended cements, are tested. Two cement types are used to prepare the samples. The oxide composition of the raw materials is given in Table 1. The cement pastes mix compositions are shown in Table 2. Note that the water-per-binder ratio W/B is expressed in mass and the replacement percentage of the additions is expressed in relation to the total amount of additions plus ordinary Portland cement (i.e. CEMI according to European nomination). Only binary systems are investigated. Note that in the case of limestone, the EN 197-1 standard accepts 35% of replacement at the most [19]. Therefore, it was decided to increase the limestone content to 40% to evaluate the consequences of such a high value.

Material	Constituent (%)									
	CaO	SiO_2	Al_2O_3	Fe_2O_3	MgO	K_2O	Na_2O	SO_3	TiO_2	LOI

CEMI 52.5 N	64.1	20.1	5.2	3.3	0.8	0.76	0.28	3.0		1.8
CEMI 52.5 N PM	60.86	19.27	4.59	3.25	2.01	0.97	0.19	2.88		1.99
Fly ash	5.08	83.45				1.66	1.4	0.58		<5
Slag	43.7	37.4	10.8	0.5	6.5	0.36	0.49	0.1	0.6	<1.5
Metakaolin	0.2	55	40	1.4	0.1	0.4	0.4	-	1.5	1

Table 1: Oxide composition of the raw materials

Mix name	W/B	Cement type	Addition type	Addition content (wt%)	Air content (vol%)
PC6	0.60	CEM I 52.5 N	-	0	0.2
FA6	0.60	CEM I 52.5 N	FA	30	0.1
SL6	0.60	CEM I 52.5 N	Slag	60	0.7
LS6	0.60	CEM I 52.5 N	Limestone	40	1.0
SL35	0.35	CEM I 52.5 N PM	Slag	50	0.1
MK45	0.45	CEM I 52.5 N	MK	20	0.1

Table 2: Mix design of the tested cement pastes

2.2 Preparation of the HCPs samples

The cement pastes are prepared using a waring blender until homogenization of the fresh mix. The pastes are poured in cylindrical molds (diameter 4 cm; height 10 cm) and vibrated to remove entrapped air bubbles. The molds are rotated for 24h in order to avoid the sedimentation of solid particles. The mixes are then demolded and stored in a 100% RH room at ambient temperature for 90 days. Note that the hydration duration is a very important parameter when studying pastes containing pozzolanic additions such as fly ash. After 90 days, it is supposed that the portlandite content of such a paste will only slightly change over a further hydration duration, since most of the pozzolanic hydration reactions have already taken place [20][21][22]. For each mix, 6 molds are prepared. The air content of each mold is determined through the density measurements of the fresh paste. Cylinders with the lowest air content are used for the diffusion tests (Table 2).

For each HCP mix, two cylinders are used for the diffusion tests before carbonation and two in the carbonated state. From these cylinders, thin samples of 2.5 mm are sawed using a precision saw. Testing thin samples is convenient since they carbonate and reach water equilibrium in a

reasonable amount of time (3 to 5 weeks). First, 60 discs are used to be tested in the non-carbonated state. These discs are placed directly in climate chambers equilibrated at three different relative humidity levels (33% 55% and 93%). The hygrometry is maintained at a constant level by means of saturated salt solutions, and soda lime was added in the climate chambers in order to avoid the carbonation of the samples during preconditioning. The CO_2 concentration inside these chambers did not exceed 10 ppm (using a sensor with a detection limit of 75 ppm). In parallel, 60 discs from the six paste mixtures are tested in the carbonated state. Carbonation of the tested samples is achieved using accelerated carbonation in an environment-controlled climate chamber equipped with a system that allows for an accurate regulation of the CO_2 partial pressure and temperature. Prior to carbonation, the 60 discs are kept in a room regulated at 55% relative humidity for a month in order to reach a constant degree of water saturation that promotes carbonation. Afterwards, they are placed in the carbonation chamber with a CO_2 content of 1 ± 0.2% for six weeks and 55%RH. This value (1% CO_2 by volume) is chosen to ensure the representativeness of the mineralogical evolution compared to atmospheric carbonation [23], to avoid cracking of cement pastes after carbonation [24] and to carbonate the samples in a reasonable amount of time. The temperature at each conditioning step is 20°C. The carbonation progress is monitored in a simple way through a phenolphthalein solution: the colorlessness of the phenolphthalein indicator test was the termination criterion. This procedure is chosen to examine samples with the same or comparable progress of carbonation. The oxygen-effective diffusion coefficient is also determined for carbonated samples at three relative humidity levels. Note that in order to test the carbonated HCP at 93% RH, all the discs are first water saturated under vacuum for 48h and placed in a climate chamber at 93%RH until mass equilibrium is reached. The reason behind water saturating these samples is to test all the HCPs in the desorption state only. After all diffusion tests are performed, the samples are dried in the oven at 105°C to reach their dry mass, which allows for the determination of their degree of water saturation at the three relative humidities chosen.

2.3 Oxygen-effective diffusion coefficient

The oxygen-effective diffusion coefficient is measured using an experimental setup developed during our previous works [9]. The test method relies on the accumulation of gaseous oxygen

inside a diffusion cell called a “downstream chamber”. The tested specimens are discs with a diameter of 4 cm and a thickness of 2.5 mm. This experimental setup contains no upstream chamber: one face of the tested specimen is in contact with the ambient air of the climate chamber (volume of 40 L), i.e. at an O_2 concentration of around 20% by volume, and the other face is in contact with the inside volume of the cell (68ml). The absence of the O_2 bottle is of relevance from a practical point of view. The volume of the climatic chamber is much larger than the volume of the downstream cell, so the oxygen concentration in the climatic chamber is constant over the test duration. At the beginning of the test, the downstream chamber is flushed with nitrogen for 20s to reach an O_2 concentration lower than 0.3%. The experimental setup (Figure 1) is then placed inside a temperature and relative humidity-controlled climate chamber (also called an “upstream chamber”).

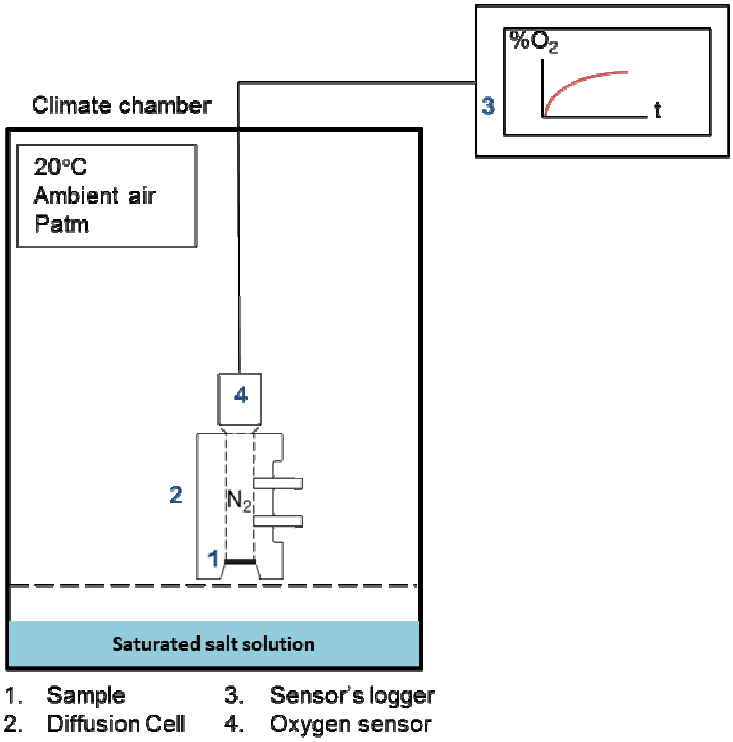

Figure 1: Schematic description of the setup of the determination of the oxygen-effective diffusion coefficient

By means of saturated salt solutions, the relative humidity inside the climate chamber is set at the same relative humidity as the one used for the pre-conditioning of the tested samples during

the diffusion test. The relative humidity level is monitored inside the climate chamber by means of a sensor during the test period and found to vary slightly (2% to 5% at the most).

Oxygen diffuses successively from the ambient air through the sample into the cell initially filled with nitrogen. Oxygen concentration is monitored inside the cell by an oxygen gas sensor. This sensor allows for continuous readings of the oxygen concentration. All measurements are carried out at 20°C and 1 atm. The oxygen-effective diffusion coefficient is determined by minimizing the residue between the experimental and numerical accumulation curve. The numerical accumulation curve is obtained by solving Fick's second law of diffusion with a finite volume solver in python called fipy, version 3.1.3 [25]. More details about the experimental setup and data analysis are given in [9].

2.4 Microstructure characterization techniques

Water porosity (ϕ) is obtained using hydrostatic weighting and oven-drying the HCP samples at 105°C. The specimens are preliminarily water-saturated under vacuum for 48h following the current standard used in France [26]. The pore size distribution of the samples is determined using mercury intrusion porosimetry (MIP). The degree of water saturation of the tested samples at 33%, 55% and 93% RH is calculated using equation (1), where m is the mass of the sample at moisture equilibrium, m_0 the dried mass, and m_{sat} the saturated mass. The saturated mass of the 2.5 mm thick samples is determined via water soaking under the vacuum for 48h. The dry mass is obtained after drying the samples in the oven at 105°C for 3 days.

$$S_r = \frac{m - m_0}{m_{sat} - m_0} \quad (1)$$

Changes in the pore structure characteristics of the paste samples after exposure to 1% CO_2 are assessed using mercury intrusion porosimetry. MIP provides information about the connectivity of the pores and reveals information about pore geometry [27]. This technique is based on the Laplace equation [28], which relates the pressure applied to the pore diameter. This diameter actually corresponds to the entry diameter of the pore. The tested samples are small blocks of a typical size of a few mm to 1 cm. These samples are cored out from the hardened cement paste

discs and pre-dried at 45°C for 24h. Note that the smallest pores (gel pores) are only partly measured by this technique. Thus, the water porosity is certainly higher [29].

Note that these tests are carried out right after sawing the thin cement pastes under water (and pre-drying at 45°C for MIP test) in order to avoid carbonation of the discs. After carbonation, when the pH-indicator becomes colorless over the 3mm thickness samples, water porosity, pore size distribution and degree of water saturation are determined on the carbonated discs. MIP test is run on one specimen only while the other tests are carried out on three replicates.

2.5 Mineralogical changes

Before and after carbonation of the HCP, one complete disc of each mix at both states is grinded and sieved completely using a sieve of 63 µm, and then 30 mg of this powder is used for the TGA and XRD tests. Only one test is run for each mix.

The mineralogical changes induced by carbonation are identified using TGA and XRD techniques. The degree of carbonation (D_oC) is determined using TGA. D_oC is defined as the CO_2-bound with respect to the total theoretical maximum binding capacity MBC (equation 4). TGA (Metller TGA-DSC 3+) is used to quantify all carbonates polymorphs. Around 30 mg of the powder sample is placed in the device and heated from 30 to 1000°C at 10°C/min under a small nitrogen flow (20 mL/min). The temperature of the carbonates' decomposition is assumed to range from 550 to 1000°C [30]. Previous work of Radha et al [31] shows that the decomposition temperature of all carbonates polymorphs is around 800°C. The samples' degree of carbonation D_oC is determined based on the amount of anhydrous cement using equations 3 and 2:

$$D_oC = \frac{BC}{MBC} \qquad (2)$$

$$B_{-CO2} = \frac{m_{CO2}^{550-1000°}}{m_{Oxyde}^{1000°C} + m_{CO2}^{0} + m_{H2O}^{0}} \qquad (3)$$

$$MBC = \sum \frac{carbonatable\ cationic\ oxide}{M(carbonatable\ cationic\ oxide)} * M_{CO2} - SO3 * \frac{M_{CO2}}{M_{SO3}} \qquad (4)$$

Where B_{-CO2} is the bound CO_2, $m_{CO2}^{550-1000°}$ is the mass loss that corresponds to the decarbonation of $CaCO_3$, m_{CO2}^{0}, and m_{H2O}^{0} are, respectively, the CO_2 and water amount present in the raw materials (cement and mineral additions used). MBC is the maximum amount of CO_2 that could be present in the sample if all CaO (except the one coming from $CaCO_3$ present in the raw materials,

and the one introduced in the mix LS6 as an additive) was carbonated. This value could be approximately inferred by the quantity of its main carbonatable cationic oxides such as CaO, MgO, SO_3, etc.

The amount of SO_3 is deduced in the calculation of the maximum degree of carbonation because in the presence of an excess of sulfate anions, calcium cations react with sulfate anions to form gypsum at room temperature even when the system is buffered by atmospheric CO_2.

The X-ray diffraction (XRD) is used to identify the nature and amount of the different calcium carbonate polymorphs. XRD tests were carried out with a Philips/PANalytical X'Pert Pro-MPD Powder Diffractometer with an X'Celerator detector of an incident CuKα radiation beam by 40 kV and 40 mA to a rotation sample. The specimens are scanned for 40 minutes from 2θ = 5 to 65° by a step of 0.25° without protection from CO_2 and in a dry environment (RH~40%).

The carbonation depths of the six HCPs are measured directly by means of phenolphthalein solution after exposing side-sealed discs of 3 cm thickness and 4 cm diameter to natural carbonation in a relative humidity controlled room at 50%. The carbonation depth is measured once a month for six months. Note that the samples were preconditioned for one week in a climate chamber with soda lime prior exposure to carbonation.

3. RESULTS

3.1 Changes in the chemical composition

The amount of portlandite, calcite and other hydration products such as C-S-H and ettringite is estimated before and after the carbonation test. The recorded mass losses during TGA are expressed in the percentage relative to the residual mass of the sample at 1000°C.

	Before carbonation (g /100g)			After carbonation (g /100g)		
Temperature range (°C)	30-350	350-550	550-950	30-350	350-550	550-950
Released component	H_2O	H_2O	CO_2	H_2O	H_2O	CO_2
Main cement phases [30]	C-S-H, AFt & other hydrates	CH	$C\bar{C}$	C-S-H, AFt & other hydrates	CH	$C\bar{C}$
PC6	18.4	9.2	4.4	10.8	7.6	36.6
FA6	16.0	5.7	4.7	5.1	0.7	33.4

SL6	15.3	4.0	3.5	5.4	0.6	30.5
LS6	12.3	6.0	21.3	4.9	1.2	51.2
SL35	14.4	5.0	4.5	5.0	0.6	27.7
MK45	19.9	4.7	4.4	5.9	0.5	24.9

Table 3: TGA results before and after carbonation of the six HCP

Table 3 presents the TGA results on the evolution of the content of bound water and CO_2 to portlandite (CH), (C-S-H), and calcium carbonate, respectively. The six HCP are tested before and after accelerated carbonation at 1%. The high content of calcium carbonate before the carbonation of the paste's LS6 corresponds to the unreacted limestone present in the initial mix, while the small amounts of calcium carbonate present in the other HCPs before carbonation are due to the initial CO_2 amount in cement (up to 2%) and to a slight carbonation of the paste during the preparation and conditioning in a CO_2-low concentration environment (10ppm). Results from Table 3 reveal that portlandite is still present only in the PC6 after carbonation, while it is consumed for blended systems.

Even though the highest amount of calcium carbonate formed after carbonation is observed for PC6, the lowest consumptions of hydration products upon carbonation are observed for this HCP.

Before carbonation (BC), results from Table 4 also reveal that a slight amount of calcite was formed during the preparation of the samples. The portlandite content of the blended cement pastes is remarkably lower than the portlandite content of PC6 because they contain less ordinary Portland cement (OPC) that can hydrate to form portlandite. Moreover, the reduced amount of portlandite formed is consumed by the pozzolanic reaction of fly ash, slag, and metakaolin.

	PC6		FA6		SL6		LS6		SL35		MK45	
	BC	C	BC	C	BC	C	BC	C	BC	C	BC	C
Calcite%	<2	9.2	<2	10.8	2.3	30	39.8	66.6	5.2	13.4	3.5	8.3
Portlandite%	18.0		7.8	4.8	5.4		8.5		4.0		6.0	
Ettringite%	<2		<2		<2		<2		<2		<2	
Vaterite%		77		57.3		57.8		13.7		56.7		78.1

Aragonite%		7.7		9		6.4				22.5		6.7

Table 4: Estimation of the content of some crystal minerals before (BC) and after carbonation (C) based on the raw data from XRD analysis

Results from Table 4 show that for all HCPs the $CaCO_3$ polymorph predominantly formed after carbonation is the metastable vaterite (vaterite is the second most metastable $CaCO_3$ polymorph after amorphous calcium carbonate [31]). Calcite and aragonite formation also took place but to a much lesser extent.

Only the samples with limestone powder showed an exception, containing mainly calcite after carbonation. The presence of limestone seems to favor the further precipitation of calcite. According to [32], calcite precipitates preferentially on limestone particles as the latter acts as a nucleation surface for calcite.

3.2 Degree of carbonation

The amount of bound-CO_2 during the preparation and the conditioning of the six HCPs (B-CO_2^{ini}), and the bound CO_2 after the carbonation test (B-CO_2^{f}) are investigated using TGA analysis (cf Table 5). These values are used to calculate the carbonation degree, expressed as the bound CO_2 per maximum bound CO_2 (MBC). Note that the amount of limestone introduced initially during the preparation of the LS6 is deducted in the calculation of the initial and final degrees of carbonation in table 5 and not deduced in the results of table 3.

Table 5 shows results of the amount of CO_2 that disappeared due to the carbonation of portlandite in the HCPs. This value (CO_2^{CH}) is calculated according de equation 5.

$$CO_2^{CH} = \left(\frac{\Delta\%CH}{M_{H2O}} M_{CO2}\right) * \frac{1}{B^{f}_{-CO2}} \qquad (5)$$

$\Delta\%CH$ (Results taken from Table 3) corresponds to the variation of the amount of water in portlandite per unit mass of anhydrous cement before and after carbonation. B^{f}_{-CO2} is the total amount of bound-CO_2 after carbonation of the HCPs (results shown in Table 5) M_{CO2} and M_{H2O} are the molar masses of carbon dioxide and water respectively. Note that the small amount of CO_2 present in the raw materials (<2%) is taken into consideration in these calculations.

The highest degree of carbonation is observed for PC6, even though the amount of bound CO_2 by portlandite is the lowest comparing to other systems, which highlights the important carbonation of other phases (C-S-H, ettringite… c.f Table 3). In agreement with this results

Meanwhile the lowest degree of carbonation is observed for SL35 (Table 5). This could be explained by the low diffusivity of the SL35 (due to the low water-binder-ratio 0.35) and its high C-S-H content. Previous works in the literature show that the carbonation of C-S-H leads to the formation of calcium-enriched silica gel. Part of the calcium would remain trapped in this gel and would not participate in the formation of $CaCO_3$ [33].

Although the phenolphthalein solution was colorless for all the six HCP after the accelerated carbonation period, the degree of carbonation of these materials varies between 34.1% and 68.4%. This result highlights the questionable reliability of the pH-indicator method to study the carbonation performance of cementitious materials. In agreement with this results, Omikrine-Metalssi et al [34] show that the carbonation continues even 1cm beyond the carbonation depth indicated by the phenolphthalein indicator. Andrade [35] also states that the DoC in the carbonated zone is not a direct function of the carbonation depth.

	MBC	B_{-CO2}^{ini}	D_OC^{ini}	B_{-CO2}^{f}	D_OC^{f}	CO_2 fixed by portlandite / Total CO_2	Amount of carbonatable compounds
	g_{CO2}/100g anhydrous	g_{CO2}/100g anhydrous	%	g_{CO2}/100g anhydrous	%	%	mol/m^3
PC6	51.2	3.1	6.1	35.3	68.4	10.7	8686.1
FA6	37.6	2	5.3	24.3	64.7	36.6	4017.4
SL6	43.1	2	4.5	21.5	49.9	27.2	2087.4
LS6	30.5	0.4	1.3	17.1	56.1	22.9	2432.1
SL35	43.4	2.4	5.5	14.8	34.1	38.8	2465.4
MK45	41.5	3.2	7.6	20.8	50.2	41.2	4773.6

Table 5: Bound CO_2 values before (B_{-CO2}^{in}) and after carbonation (B_{-CO2}^{f}); carbonation degrees of the tested material before (D_oC^{ini}) and after carbonation (D_oC^{f}); maximum CO_2-binding capacity (MBC), and the amount of carbonatable compounds of the six HCPs

Note that the amount of carbonatable compounds is deduced from the final bound-CO_2 by multiplying this value with the cement dosage and dividing by the molar mass of carbon dioxide. This property is a direct input parameter required by service life prediction models (equation (6)).

3.3 Porosity changes upon carbonation

Figure 2 gives the porosities of the six HCPs before and after carbonation. The total water porosity of the carbonated cement pastes is 6 to 12% smaller than the total porosity of HCPs before carbonation. The carbonation of the hydrates phases in cement is known to cause an increase in the solid phase volume.

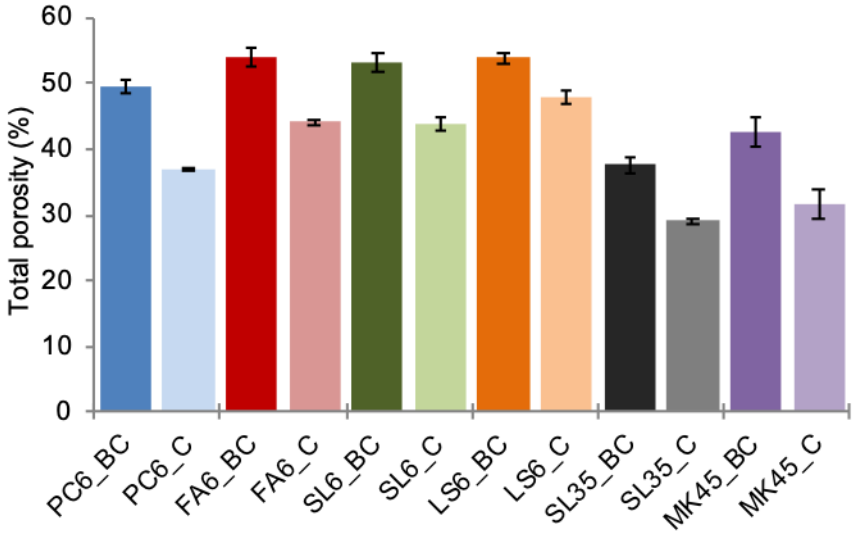

Figure 2 : Influence of carbonation on the water porosity of the six HCPs. BC: before carbonation C: carbonated.

Although FA6, SL6, and MK45 contain a large amount of C-S-H, their total porosity decrease was lower than PC6. This could be due to the smaller molar volume (change due to carbonation) of low Ca/Si C-S-H in HCPs with pozzolanic additions, which generally causes a slight decrease in the porosity [36]. The effect of carbonation on the six HCPs' pore size distribution (PSD) is investigated by means of MIP (Figure 3). It is noted that for PC6 carbonation resulted in a reduction of the amount of small pores (d<8 nm) and a formation of a large amount of pores with a bigger diameter than 20 nm. The carbonation of the paste FA6 even induced the disappearance of pores with a small diameter < 10 nm and the formation of pores with a diameter of 200 nm. Note that this paste pore size distribution goes from a bimodal distribution to a trimodal distribution upon carbonation. This result is also observed for the pastes' SL6; the pore size distribution goes from a monomodal distribution centered on pores with a diameter of 10 nm to a bimodal distribution of higher pore diameter: 60 and 30 nm. A coarsening in the pore size distribution of LS6 is observed: carbonated LS6 contains a lower number of small pores and a shift of the main mode to a bigger pore diameter

is observed. As for SL35, carbonation caused the formation of small pores with a diameter of around 3 nm, the clogging of pores with a diameter of around 7 nm, and an increase in the pores entry diameter. This result is also observed on MK45, where carbonation caused a clogging of pores with a diameter of 20 nm and an appearance of a small amount of pores with a bigger diameter of 40 nm after carbonation.

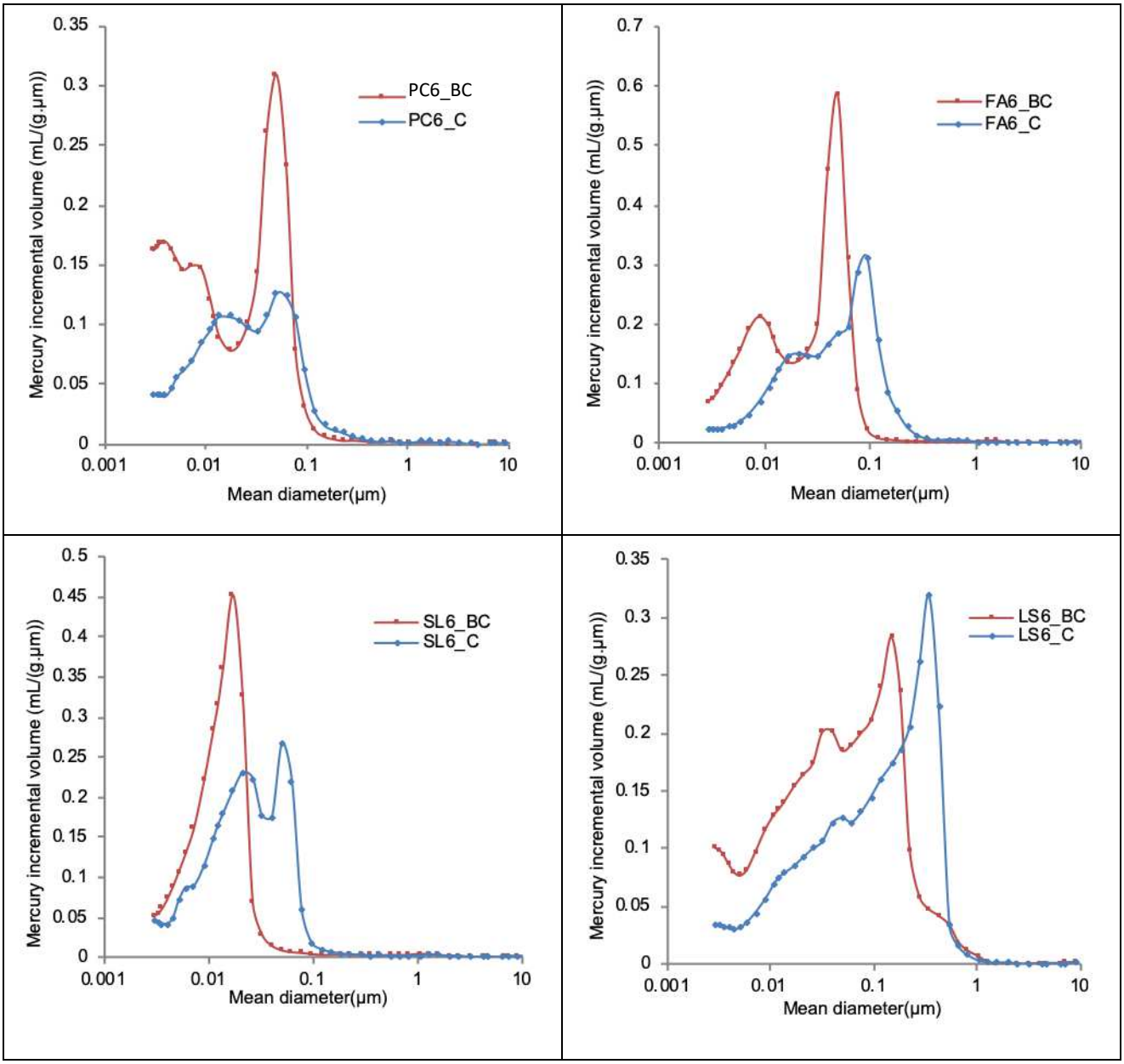

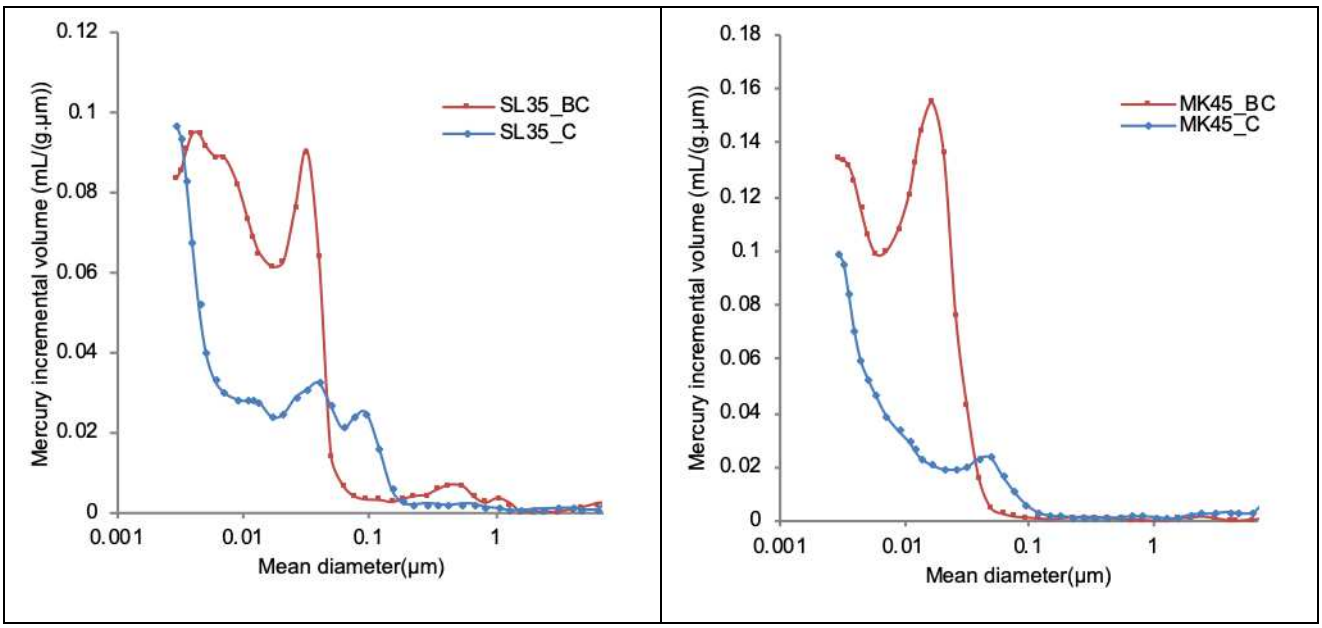

307 Figure 3 : MIP results on the PSD of the six HCPs before carbonation (BC) and after carbonation

308 (C)

309 *3.4 Effect of carbonation on the water retention capacity*

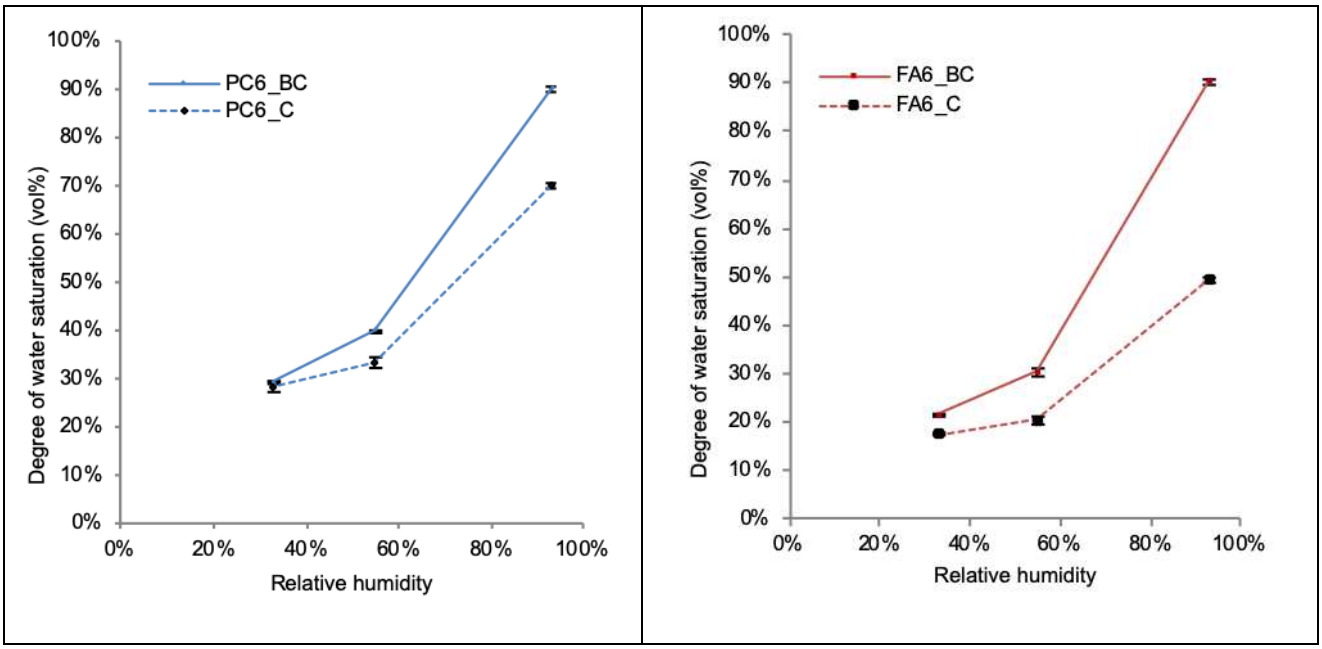

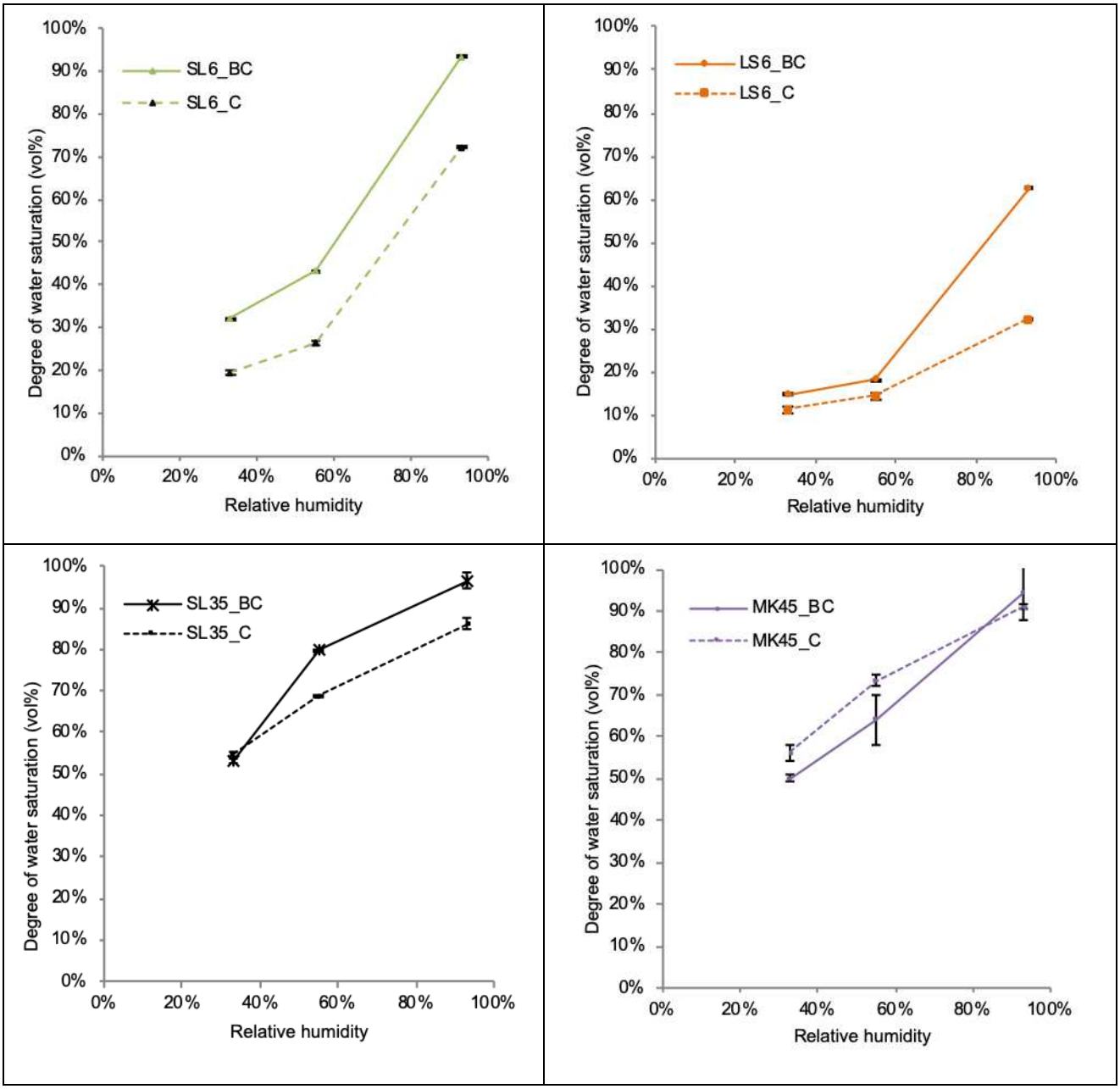

Figure 4: The degree of water saturation (vol%) of the tested HCPs before carbonation (BC) and after carbonation (C) at three relative humidity levels

Results shown in Figure 4 indicate that carbonation exerts a different effect on the water retention capacity of the hardened cement pastes. For pastes PC6, FA6, LS6 and SL35, the degree of water saturation at 33%RH only slightly changed; however, at 55% RH, carbonated samples are 3% to 17% less water saturated and at 93% RH, carbonated samples are 11% to 41% less water saturated. As for SL6, carbonated samples are 20% less water saturated at almost all relative humidity levels; however, carbonated MK45s are 6% to 9% more water saturated than the non-carbonated samples at 33% and 55% RH, and only 3% less water saturated at 93% relative humidity. Note that the decrease in the water retention capacity upon carbonation is investigated in

the first desorption isotherm (from water saturated condition) and is more significant for blended cement pastes and appears to be all the more significant as the amount of additions and the water-per-binder ratio are high (SL6).

3.5 Effect of carbonation on oxygen-effective diffusion coefficient

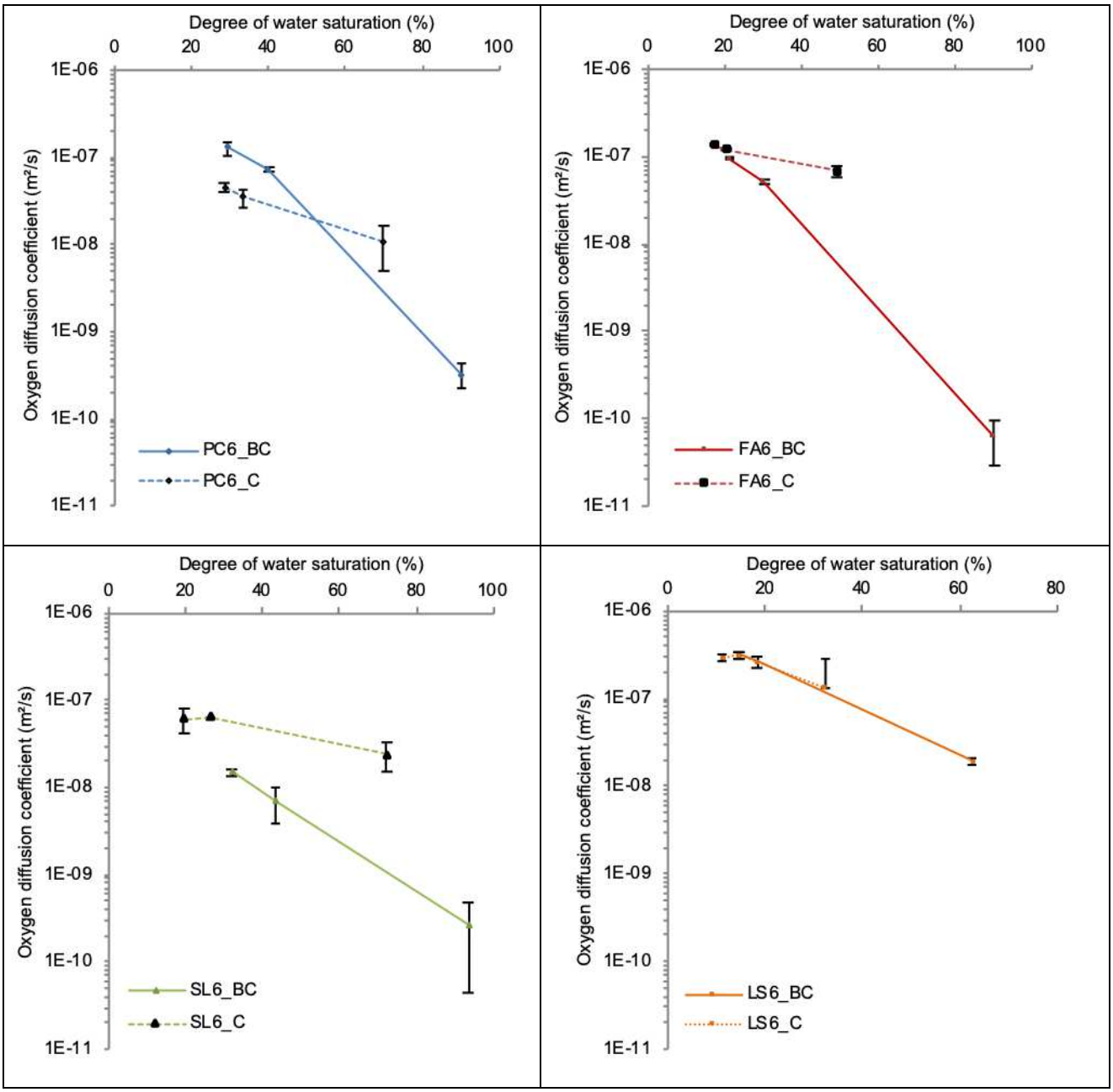

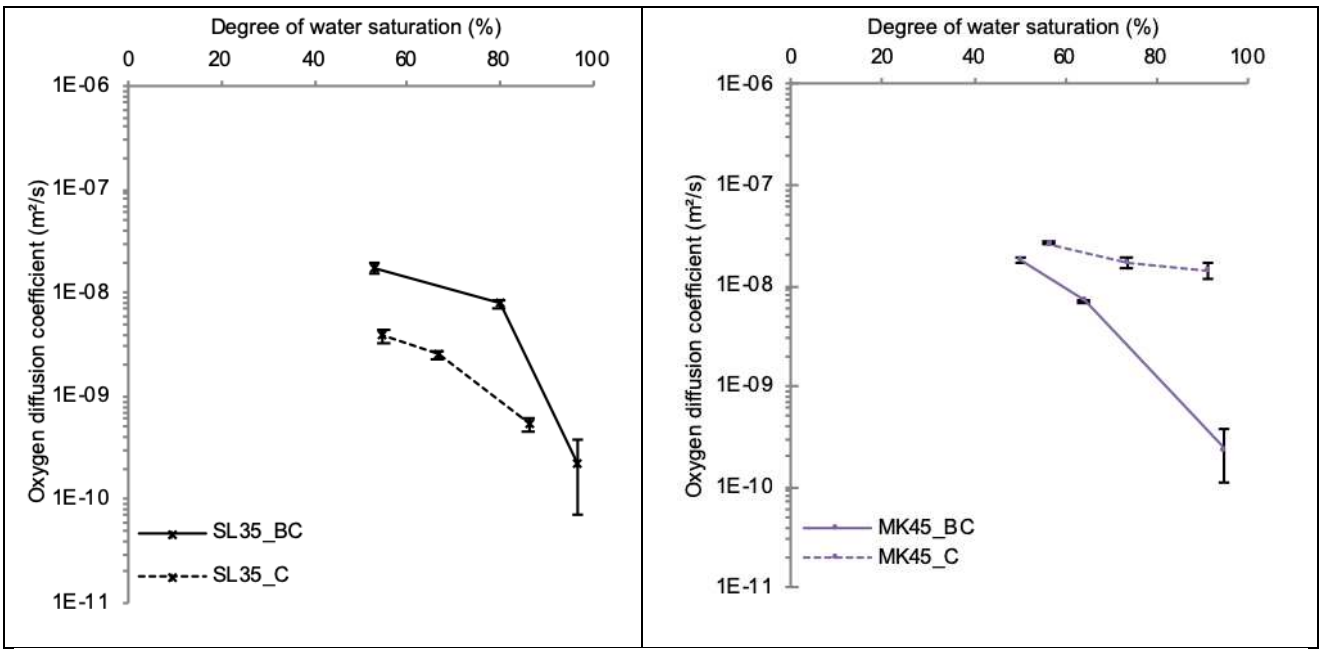

Figure 5: Oxygen-effective diffusion coefficient of the tested HCPs before and after carbonation at three degrees of water saturation

The oxygen-effective diffusion coefficient depends both on the degrees of water saturation corresponding to the relative humidity of preconditioning and on the state of carbonation (Figure 5). PC6 pastes exhibit a decrease in the oxygen-effective diffusion coefficient by a factor of 3 at low and intermediate relative humidity upon carbonation, whereas an increase in $D_{e,O2}$ by a factor of 21 at 93% RH is observed upon carbonation. The same is observed for SL35: $D_{e,O2}$ decreased by a factor of 5 and 3 at 33% and 55% RH, respectively, and increased by a factor of 2.5 at 93% RH.

As for FA6 pastes, carbonation caused an increase in the $D_{e,O2}$ at all relative humidity levels by a factor of 1.5, 2.3 and 1000 at 33%, 55% and 93% RH, respectively. $D_{e,O2}$ also increased for SL6 by a factor of 4, 9 and 93 at 33%, 55% and 93% RH, respectively. For LS6, $D_{e,O2}$ is hardly influenced by carbonation at 33% and 55% RH while it increased by a factor of 7 at a high RH of 93%. Note that LS6 diffusivity before carbonation is the highest. Carbonated MK45 exhibits higher oxygen diffusivity at all RH levels. $D_{e,O2}$ increases by a factor of 1.5, 2.3 and 60 at 33%, 55% and 93% RH, respectively. Note that the oxygen-effective diffusion coefficient is highly dependent on the relative humidity of preconditioning for non-carbonated HCPs and only slightly dependent on the RH of carbonated HCPs.

4. DISCUSSION

342 *4.1 Microstructural changes upon carbonation*

343 The decrease in the total porosity given in the results (Figure 2) is also noticed by several authors
344 in the literature [37][11], either on-site [38][39] or under accelerated exposure conditions [40][41].
345 Pihlajavaara et al [42] and Tri et al [41] measured a decrease in the total porosity (clogging)
346 ranging from 10% to 15% on CEMI-based carbonate cement pastes (0.3 <W/C <0.8). Figure 2
347 shows that the nature of the binder is involved in the variation of porosity; the highest porosity
348 change is found for PC6 (12%). In agreement with our findings, Hyvert [43] also found that the total
349 porosity variation is more important for CEMI (9.4%) materials than CEMIII (6%) materials. This
350 result could be directly linked to the nature and relative amount of the hydrates formed by
351 pozzolanic reactions that lower the amount of portlandite and that lower the Ca to Si ratio in C-S-H
352 phases, as the high content of C-S-H tends to maximize this drop in porosity [11]. Note that FA6
353 total porosity is 5 to 7% higher than the total porosity of PC6. This result was also obtained by
354 Papadakis el al [44] when testing mortar samples prepared with 30% fly ash, an increase in
355 porosity of 13% is found.

356 The pore size distribution is also strongly impacted by carbonation (cf. Figure 3). When the W/B is
357 high, which is the case of the HCPs PC6, SL6, and LS6, the carbonation caused a coarsening of
358 the PSD. However, for SL35 and MK45, carbonation resulted in the formation of both finer and
359 coarser pores. Johannesson and Utgenannt [45] also reported a redistribution of pore sizes upon
360 carbonation in Portland cement mortar samples. The authors predicted that well-carbonated mortar
361 has a significantly higher volume of pores in the pore size range of 2 to 7 nm. Those MIP results
362 are also consistent with the observations of Shah et al [10].

363 As a consequence of the variation in the pore size distribution and porosity of the HCPs upon
364 carbonation, the water retention capacity decreased notably (Figure 4). These results are
365 explained, together with the overall evolution of pore size distribution, by the consumption of the C-
366 S-H phase after carbonation and the increase of pore entry diameter. In agreement with our
367 results, it has been reported by Johannesson and Utgenannt [45] that the degree of water
368 saturation (obtained by desorption) for the non-carbonated mortars is higher (by 15%) when
369 compared with a well-carbonated sample, especially at 95% relative humidity. The reduction of
370 liquid saturation (S_l) is observed in spite of the reduction of total porosity (ϕ), which means that the

371 average volume content of water per unit volume of paste decreases but the pore entry diameter
372 tends to increase upon carbonation.

373 *4.2 Mineralogical changes*

374 Tables 3, 4, and 5 results show that after carbonation, portlandite is still present in carbonated PC6
375 (only 10% of bound-CO_2 was due to carbonation of portlandite) while it is highly consumed for
376 blended cement pastes. In agreement with our findings, Soja et al [37] determined a higher
377 portlandite consumption for blended cements with limestone with regards to OPC pastes after
378 exposure to natural carbonation, which is a rather encouraging result for predicting the natural
379 carbonation mechanisms from accelerated carbonation tests at 1% CO_2. MK45, which contains
380 20% metakaolin, also showed an almost complete depletion of portlandite (41% of the total bound-
381 CO_2 is due to portlandite carbonation Table 5) and a high consumption of C-S-H after carbonation
382 at 1% CO_2 (cf Table 3). The same conclusion is drawn by Machner et al [46], who noted that
383 carbonation caused an almost complete decomposition of the C-S-H phase and the consumption
384 of the portlandite after carbonation at 1% CO_2 of HCPs with 20% metakaolin. XRD results (Table 4)
385 show the formation of the three $CaCO_3$ polymorphs for all HCPs with a high amount of calcite for
386 LS6 and a predominant formation of vaterite for other HCP. The high formation of vaterite could be
387 explained by the carbonation of C-S-H phases. Indeed, Black et al [47][48] studied the carbonation
388 of synthetic C-S-H in which the initial Ca/Si ratio appeared to influence the crystalline carbonate
389 species formed. For Ca/Si ratios greater than 0.67, principally calcite and vaterite were observed
390 and for ratios below 0.50, aragonite was most prevalent. Thiery et al. [49] attributed the more
391 poorly crystallized and the more thermodynamically unstable forms of $CaCO_3$ to the carbonation of
392 the C-S-H phases.

393 *4.3 Oxygen-effective diffusion coefficient*

394 The pronounced reduction in the total porosity as a result of carbonation (precipitation of
395 calcium carbonates causes clogging of total porosity) of the six HCPs is expected to positively
396 affect the durability performance of the materials, thus reducing the oxygen-effective diffusion
397 coefficient. This is indeed observed for PC6, LS6 and SL35 at 33% and 55% RH. This reduction
398 could be explained by the fact that carbonation only slightly varied the degree of water saturation at

these two RH levels (3 to 8%). However, at a high relative humidity of 93%, the O_2-effective diffusion coefficient for carbonated samples decreased notably by a factor that varies from 2.4 (SL35) to 10 (LS6). This result is a consequence of the decrease of the water retention capacity of these HCPs after carbonation (cf. Figure 4). An increase in the diffusion coefficient is obtained after the carbonation of FA6 and SL6 because of the low degree of water saturation of these samples upon carbonation (cf. Figure 4). In agreement with our results, Dutzer et al [24] show an increase in the gaseous helium diffusivity upon accelerated carbonation (3% CO_2 vol.) for blended cement pastes, a result they attributed to the cracking induced carbonation.

However, $D_{e,O2}$ results of MK45 are inconsistent: although the degree of water saturation slightly increased upon carbonation (Figure 4) and MIP results showed the formation of small porosity for carbonated samples (Figure 3), the oxygen-effective diffusion coefficient increased at all RH levels (factor up to 60 at 93% RH). This result could be explained by the slight increase of the largest pore diameter, even if its volume fraction is lowered (Figure 3). Note that the oxygen-effective diffusion coefficient of the six HCPs after carbonation is less dependent on the RH of preconditioning compared to the non-carbonated state diffusivity. *Soja* et al [37] investigated the influence of natural carbonation on the oxygen-effective diffusion coefficient on CEMI and limestone blended cement pastes. Results show a lower oxygen-effective diffusion coefficient even for limestone blended samples equilibrated at 70% RH. Houst et al [42] noted that the carbonation of Portland cement paste samples caused a decrease in the diffusivity of CO_2 and O_2 at intermediate RH. These microstructural modifications strongly modify the transfer properties in cementitious materials, especially in terms of diffusion and permeability. However, we noticed that this conclusion is only valid for PC6, LS6 and SL35 at low and intermediate relative humidity levels. Our results on the variation of $D_{e,O2}$ upon carbonation for the six HCPs can be summarized as follows: (i) for blended cement pastes with a W/B 0.45 and 0.6, an increase of the gas diffusivity is observed at all RH levels, (ii) PC6 and SL35 show a decrease in the diffusion coefficient at 33% and 55% RH and an increase in the $D_{e,O2}$ at 93% RH, (iii) for all HCP (but LS6), $D_{e,O2}$ is less dependent on the RH in the carbonated state.

4.4 Gas-diffusivity versus mean pore diameter

Using an automatic tool that allows for the fitting of the data from the MIP analysis (Figure 3), the mean pore diameter and its corresponding volumetric fraction is computed assuming that each mode is of a normal distribution (Figure 6). This analysis is carried out for all HCPs before and after carbonation. The number of modes of each MIP result is chosen in order to optimize the fit.

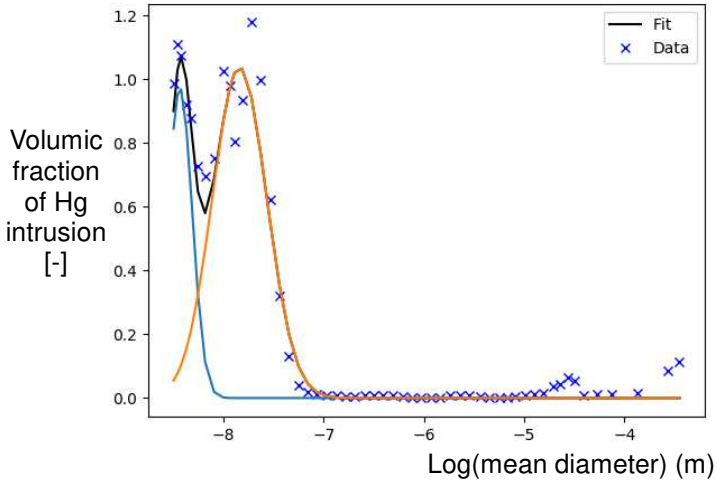

Figure 6: An example of MIP data automatically fitted

Using these results, a weighted arithmetic mean (the weight in the volumetric fraction of each mode) diameter of each paste MIP data (Figure 3) is calculated and compared with the effective-diffusion coefficients determined experimentally on samples with a saturation degree lower than 50%. The oxygen-effective diffusion coefficient is corrected by the total porosity (ϕ) and the degree of water saturation (S_l) of the tested samples. This correction is made in order to consider that the transport process is made only through the gas filled pores.

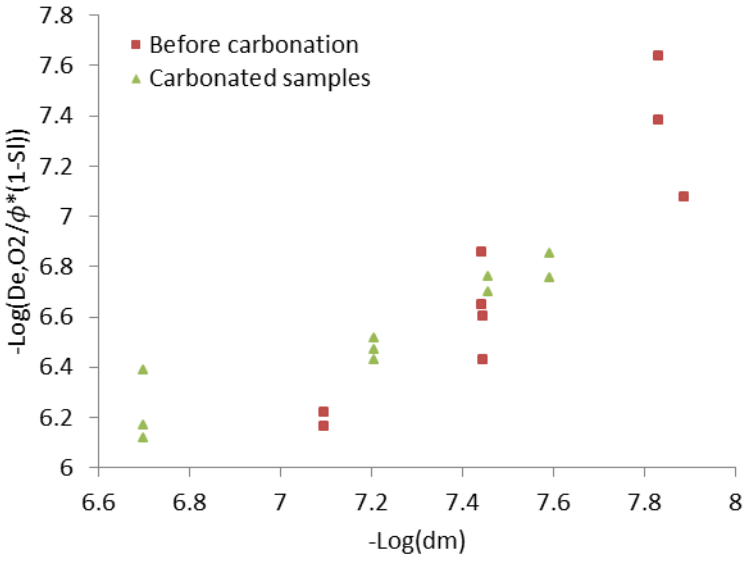

Figure 7: Oxygen-effective diffusion coefficient versus weighted mean pore diameter at different of saturation degrees

Under the Knudsen diffusion assumption, the effective diffusion coefficient is directly proportional to the mean pore diameter of the cementitious material when the mean pore diameter is lower than the mean free path of oxygen molecules at atmospheric pressure and 20^0C (i.e. $-\log(d_m)>7$) [50][51]. Indeed, Figure 7 shows that the oxygen-effective diffusion coefficient displays a somewhat linear trend (in log-scale) with respect to the weighted mean pore diameter ($-\text{Log}(d_m) > 7$). For carbonated and non-carbonated samples, the slope equals 0.9±0.05 (R^2 = 0.92) and 1.6±0.2 (R^2 = 0.84), respectively. These results show that the pore size distribution and the degree of water saturation are appropriate material properties to consider in the modeling of the gas-diffusivity of cementitious materials. Note that this result is consistent with previous findings in the literature [9] carried out on HCPs hydrated at different durations.

4.5 Carbonation performance of different HCPs

The carbonation rate (mm/year$^{0.5}$) of the tested HCPs is calculated at 55% RH from the results of oxygen gas diffusivity at the carbonated state (Figure 5) and TGA results of the amount of carbonatable compounds (Table 5). Note that the amount of carbonatable compounds is the product of the cement dosage in the paste by the CO_2-binding capacity. This 55% relative humidity is chosen since it is suggested that the most rapid carbonation of concrete occurs at a relative humidity near 50% to 65%, which is also the recommended RH for natural carbonation tests by the EN 12390-10 standard [19]. The carbonation depth (Xc) of these HCPs are calculated based on the Papadakis deterministic model [5] (equation 6), where $[CO2]_0$ is the ambient CO_2 concentration (400±25ppm) converted to mol.m^{-3}, t is the carbonation exposure duration (s), $D_{e,CO2}$ the CO_2-effective diffusion coefficient in the carbonated layer, and carbonatable compounds (mol.m^{-3}). Note that $D_{e,CO2}$ is calculated using Graham's law, which allows it to be deduced from the O_2-effective diffusion coefficient.

$$x_c = \sqrt{\frac{2\, D_{e,CO2}\, [CO2]_0}{Carbonatable\ compounds} \cdot t} \qquad (6)$$

SL35 results are not shown on Figure 8 because no sharp carbonation depth could be seen on these samples even after 4 months of exposure.

HCP	Carbonation kinetics (mm/year$^{0.5}$)
PC6	1.7
FA6	4.6
SL6	4.7
LS6	9.6
SL35	1
MK45	1.6

Table 6 : Carbonation kinetics calculated under natural carbonation (400 ppm) carbonation at 55% RH

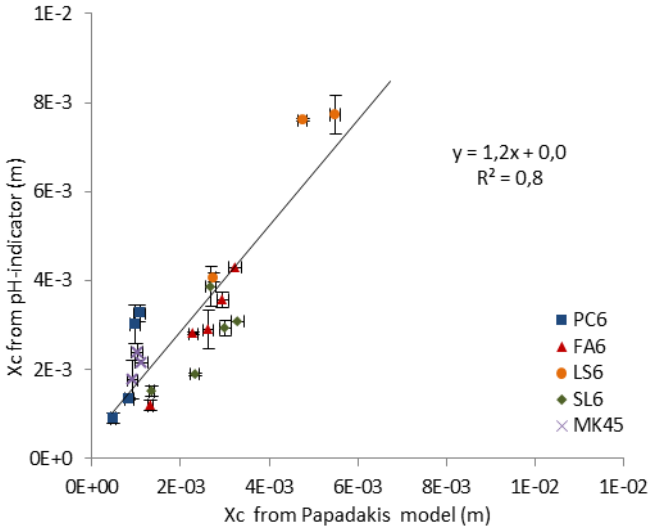

Figure 8: HCPs' Xc determined with pH-indicator vs Xc predicted using Papadakis' model

Figure 8 shows that the carbonation depths obtained from Papadakis' model are correlated to the carbonation depths measured experimentally using phenolphthalein solution. The horizontal error bars are due to oxygen-effective diffusion coefficient variation within replicates, and the vertical errors bars are a result of averaging 5 carbonation depth readings. The pH-indicator results are slightly higher than Papadakis' model; this overestimation could be due to errors of averaging or microcracks within the samples (that the model does not take into consideration).

As expected, PC6 and blended HCPs with low W/B ratios (SL35 and MK45 cf. Table 6) present the highest carbonation resistance. These results are explained by the very low gas diffusion coefficient of the SL35 and MK45 and PC6's high amount of carbonatable compounds. Although PC6 contains the highest carbonatable compounds, SL35 and MK45 have a higher carbonation resistance (i.e. lower carbonation kinetics). These results show that the carbonation depth progression is mainly driven by the CO_2-effective diffusion coefficient of these pastes: the gas-diffusivity of SL35 and MK45 is 10 and 2 times lower than for PC6, respectively. Therefore, the low value of gas diffusivity can compensate for the low carbonatable compounds content. FA6,

482 containing 30% fly ash, showed low carbonation resistance (high carbonation kinetics of 4.6
483 mm/year$^{0.5}$). Fly ash is known to react with the calcium hydroxide CH formed during the hydration
484 of the cement to form calcium silicate hydrate C-S-H with a lower C/S ratio [36] than the C-S-H
485 phase in pure Portland cement. Indeed, various studies in the literature found increased
486 carbonation depths of concrete when adding fly ash. Morandeau et al [52] reported that with
487 increasing clinker by fly ash (0%, 30%), the carbonation depth under accelerated carbonation (10%
488 CO_2, 63% RH) increases by a factor of 2. SL6 and SL35 with 60% and 50% slag replacement by
489 mass, respectively, contain a comparable amount of carbonatable compounds because of the
490 similar cement composition. In spite of that, SL6 carbonation resistance is almost 5 times higher
491 than SL35 (cf. Table 6). This is due to the low W/B ratio of SL35, which caused the oxygen-
492 effective diffusion coefficient of SL35 to be 26 times lower than SL6. In comparison to PC6, SL6,
493 which is cast at the same W/B (0.6), has a carbonation kinetic that is 2.8 times higher. This is
494 explained by the low carbonatable compounds of SL6 compared to PC6 (cf. Table 5). Furthermore,
495 HCPs containing slag have a C-S-H phase with a C/S ratio around 1.5 and below [53]. LS6
496 performed the worst concerning carbonation resistance. This is due to the high limestone
497 substitution level (40%), low carbonatable compounds, and high oxygen-effective diffusion
498 coefficient in both carbonated and non-carbonated states. The latter is due to the coarser pore
499 structure compared to pure Portland cement (PC6) (cf. Figure 3), which is characterized by larger,
500 interconnected pores. Such a pore structure promotes gaseous CO_2 transport. The high
501 carbonation kinetics of limestone cement pastes is also justified with the fact that calcite forms
502 preferentially on limestone particles, and less on portlandite and the C-S-H phases [32][54]. The
503 latter would prevent their further carbonation or slow it down considerably. Lollini et al [55] reported
504 that with a limestone content of 15%, no influence on the carbonation behaviour was observed, but
505 at 30%, a remarkable worsening of the carbonation resistance is observed (by 60% to 80%). The
506 MK45 carbonation rate is found to be comparable to that of PC6, although the latter is cast at a
507 W/B ratio of 0.6 and the MK45 W/B ratio is 0.45, and MK45 carbonatable compounds is twice
508 lower than PC6. Note that MK45 gas diffusivity is two times lower than PC6, which compensates
509 for the lower amount of carbonatable compounds in MK45 pastes. Bucher et al [56] investigated
510 the natural and accelerated carbonation (4% CO_2) of concrete specimen with a cement

511 replacement of 15 to 25% metakaolin cast at a water per binder ratio of 0.6. In this case, the
512 carbonation depth of concrete with metakaolin is found to be 2 to 4 times higher than the
513 carbonation depth of concrete specimen with CEMI: the higher the metakaolin content, the greater
514 the carbonation depth.

515 **CONCLUSIONS**

516 The results of this work allow drawing the following conclusions:

517 • Despite a porosity clogging, carbonation induces an increase in the oxygen-effective
518 diffusion coefficient for most of the tested HCPs at all relative humidity levels. Only the
519 Portland cement paste with W/B=0.6 and the slag paste with W/B=0.35 have a decreased
520 gas diffusivity at 33% and 55% RH after carbonation.

521 • The oxygen-effective diffusion coefficient variation upon carbonation at a given RH is
522 explained by changes in both the water retention capacity and the pore size distribution.

523 • For all HCPs, the oxygen-effective diffusion coefficient is less dependent on the relative
524 humidity of preconditioning after carbonation than before.

525 • The gas diffusion coefficient shows a good correlation with the mean pore diameter of the
526 tested HCPs (in log scale) when the degree of water saturation is lower than 50%. This
527 result is established for both carbonated and non-carbonated HCPs, which proves the
528 direct dependence of the gas diffusivity on the pore size distribution and degree of water
529 saturation of cementitious materials.

530 • Regarding the durability performance, the theoretical carbonation rate should be dominated
531 by the gas diffusivity, since, for the tested HCPs, the latter varies over two orders of
532 magnitude, while the amount of carbonatable compounds varies only by a factor of 4.

533 • Materials made with a combination of OPC, slag or metakaolin could behave as well as
534 material containing only OPC with respect to carbonation, providing a low gas diffusivity
535 which can be obtained by a W/B ratio carefully optimized. This could provide a real
536 opportunity to decrease the clinker content in concretes without impacting negatively the
537 durability performance related to carbonation. Further studies on the reinforcement

corrosion rate using this kind of mixtures must be carried out before definite conclusion can be made.

No conflict of interest

The authors declare that they have no conflict of interest.

Acknowledgements

The authors would like to thank LafargeHolcim research center and the Association Nationale de la recherche et de la Technologie for the funding of this research. The authors gratefully acknowledge the technical help of Alain CHONIER, Gabriel PHAM, and the analytical support team of LafargeHolcim research centre.

REFERENCES

[1] W. Ashraf, Carbonation of cement-based materials: Challenges and opportunities, Constr. Build. Mater. 120 (2016) 558–570.

[2] P. Turcry, L. Oksri-Nelfia, A. Younsi, A. Aït-Mokhtar, Analysis of an accelerated carbonation test with severe preconditioning, Cem. Concr. Res. (2014).

[3] O. Omikrine Metalssi, A. Aït-Mokhtar, P. Turcry, B. Ruot, Consequences of carbonation on microstructure and drying shrinkage of a mortar with cellulose ether, Constr. Build. Mater. 34 (2012) 218–225.

[4] B. Šavija, M. Luković, Carbonation of cement paste: Understanding, challenges, and opportunities, Constr. Build. Mater. 117 (2016) 285–301.

[5] V.G. Papadakis, C.G. Vayenas, M.N. Fardis, A reaction engineering approach to the problem of concrete carbonation, AIChE J. 35 (1989) 1639–1650.

[6] International Federation for Structural Concrete, MC-SLD:2006. Model Code for Service Life Design, in: Model Code Bull. 34, 2006: p. 116.

[7] C. Thiel, C. Gehlen, Compliance testing for probabilistic durability design purposes, in: Sixth Int. Symp. Life-Cycle Civ. Eng. (IALCCE 2018), Ghent, Belgium, 2018.

[8] H.S. Wong, N.R. Buenfeld, M.K. Head, Estimating transport properties of mortars using image analysis on backscattered electron images, Cem. Concr. Res. 36 (2006) 1556–1566.

[9] M. Boumaaza, B. Huet, G. Pham, P. Turcry, A. Aït-Mokhtar, C. Gehlen, A new test method to

566 determine the gaseous oxygen diffusion coefficient of cement pastes as a function of
567 hydration duration , microstructure , and relative humidity, Mater. Struct. 51 (2018) 1–31.
568 [10] V. Shah, K. Scrivener, B. Bhattacharjee, S. Bishnoi, Changes in microstructure
569 characteristics of cement paste on carbonation, Cem. Concr. Res. 109 (2018) 184–197.
570 [11] M. Auroy, S. Poyer, P. Le Bescop, J. Torrenti, T. Charpentier, M. Moskura, X. Bourbon,
571 Impact of carbonation on unsaturated water transport properties of cement-based materials,
572 Cem. Concr. Res. 74 (2015) 44–58.
573 [12] H. Jansson, R. Snibb, K. Bohlin, I. Lofgren, Carbonation of concrete with mineral additions,
574 in: Proc. XXIII Nord. Concr. Res. Symp., Aalborg, Denmark, 2017: pp. 101–104.
575 [13] N. Issaadi, A. Nouviaire, R. Belarbi, A. Aït-Mokhtar, Moisture characterization of cementitious
576 material properties : Assessment of water vapor sorption isotherm and permeability variation
577 with ages, Constr. Build. Mater. 83 (2015) 237–247.
578 [14] J. Sercombe, R. Vidal, C. Gallé, F. Adenot, Experimental study of gas diffusion in cement
579 paste, Cem. Concr. Res. 37 (2007) 579–588.
580 [15] O. Amiri, A. Aït-Mokhtar, M. Sarhani, Tri-dimensional modelling of cementitious materials
581 permeability from polymodal pore size distribution obtained by mercury intrusion porosimetry
582 tests, Adv. Cem. Res. 17 (2005) 39–45.
583 [16] S. Peng, Q. Hu, S. Hamamoto, Diffusivity of rocks: Gas diffusion measurements and
584 correlation to porosity and pore size distribution, Water Resour. Res. 48 (2012) 1–9.
585 [17] A. Leemann, R. Loser, B. Münch, P. Lura, Steady-state O2 and CO2 diffusion in carbonated
586 mortars produced with blended cements, Mater. Struct. 50 (2017) 50:247.
587 [18] C. Andrade, A.S. Miguel, Updating Carbon Storage Capacity of Spanish Cements, Sustain.
588 10 (2018) 4806.
589 [19] EN 197-1, Cement Part 1: Composition, Specifications and Conformity Criteria for Common
590 Cements, Br. Stand. (2011).
591 [20] E.M.J. Berodier, Impact of the Supplementary Cementitious Materials on the kinetics and
592 microstructural development of cement hydration, PhD thesis. Ecole polytechnique federale
593 de lausanne, 2015.
594 [21] C. Naber, S. Stegmeyer, D. Jansen, F. Goetz-Neunhoeffer, J. Neubauer, The PONKCS

595 method applied for time resolved XRD quantification of supplementary cementitious material
596 reactivity in hydrating mixtures with ordinary Portland cement, Constr. Build. Mater. 214
597 (2019) 449–457.
598 [22] A.K. Schindler, K.J. Folliard, Influence of supplementary cementing materials on the heat of
599 hydration of concrete, in: Adv. Cem. Concr. IX Conf., Colorado, 2003: pp. 10–14.
600 [23] M. Auroy, S. Poyet, P. Le Bescop, J.M. Torrenti, T. Charpentier, M. Moskura, X. Bourbon,
601 Comparison between natural and accelerated carbonation (3% CO2): Impact on mineralogy,
602 microstructure, water retention and cracking, Cem. Concr. Res. 109 (2018) 64–80.
603 [24] V. Dutzer, W. Dridi, S. Poyet, P. Le Bescop, X. Bourbon, The link between gas diffusion and
604 carbonation in hardened cement pastes, Cem. Concr. Res. 123 (2019) 105795.
605 [25] J.E. Guyer, D. Wheeler, J.A. Warren, FiPy: Partial differential equations with python,
606 Comput. Sci. Eng. 11 (2009) 6–15.
607 [26] Association Française de Normalisation (AFNOR), Determination of real and apparent
608 densities, open and total porosities, in: AFNOR (Ed.), NF EN 1936, 2007.
609 [27] E. Berodier, K. Scrivener, Evolution of pore structure in blended systems, Cem. Concr. Res.
610 73 (2015) 25–35.
611 [28] O. Coussy, Surface Energy and Capillarity, in: Mech. Phys. Porous Solids, John Wiley, 2010:
612 pp. 121–122.
613 [29] A. Abell, K. Willis, D. Lange, Mercury Intrusion Porosimetry and Image Analysis of Cement-
614 Based Materials., J. Colloid Interface Sci. 211 (1999) 39–44.
615 [30] N.C. Collier, Transition and decomposition temperatures of cement phases – a collection of
616 thermal analysis data, Ceramics-Silikaty. 60 338-343 (2016).
617 [31] A. V. Radha, T.Z. Forbes, C.E. Killian, P.U.P.A. Gilbert, A. Navrotsky, Transformation and
618 crystallization energetics of synthetic and biogenic amorphous calcium carbonate, Proc.
619 Natl. Acad. Sci. 107 (2010) 16438–16443.
620 [32] Q. Tri, N. Maes, D. Jacques, E. Bruneel, I. Van Driessche, G. Ye, G. De Schutter, Effect of
621 limestone fillers on microstructure and permeability due to carbonation of cement pastes
622 under controlled CO2 pressure conditions, Constr. Build. Mater. 82 (2015) 376–390.
623 [33] K. Suzuki, N. Tadahiro, S. Ito, Formation and carbonation of CSH in water, Cem. Concr.

Res. 15 (1985) 213–224.

[34] O. Metalssi, A. Aït-Mokhtar, A proposed methodology for a quantitative investigation of carbonation in polymer-modified mortars, Exp. Tech. 33 (2009) 59–65.

[35] C. Andrade, Evaluation of the degree of carbonation of concretes in three environments, Constr. Build. Mater. 230 (2020) 116804.

[36] A. Morandeau, M. Thiéry, P. Dangla, Investigation of the carbonation mechanism of CH and C-S-H in terms of kinetics, microstructure changes and moisture properties, Cem. Concr. Res. 56 (2014) 153–170.

[37] W. Soja, H. Maraghechi, F. Georget, K. Scrivener, Changes of microstructure and diffusivity in blended cement pastes exposed to natural carbonation, in: MATEC Web Conf. ICCRRR, Cape Town, South Africa, 2018: p. 199.

[38] S.E. Pihlajavaara, Some results of the effect of carbonation on the porosity and pore size distribution of cement paste, Mater. Struct. (1968) 521–527.

[39] S.E. Pihlajavaara, P. Esko, Effect of carbonation on microstructural properties of cement stones, Cem. Concr. Res. 4 (1974) 149–154.

[40] V. Papadakis, C. Vayenas, M. Fardis, Physical and chemical characteristics affecting the durability of concrete, ACI Mater. J. 8 (1991) 186–196.

[41] V. Ngala, C. Page, Effect of carbonation on pore structure and diffusional properties of hydrated cement pastes, Cem. Concr. Res. 27 (1997) 995–1007.

[42] Y. Houst, F.H. Wittmann, Influence of porosity and water content on the diffusivity of CO2 and O2 through hydrated cement paste, Cem. Concr. Res. 24 (1994) 1165–1176.

[43] N. Hyvert, Application de l'approche probabiliste à la durabilité des produits préfabriqués en béton, PhD thesis. Université de Toulouse, 2009.

[44] V.G. Papadakis, Effect of supplementary cementing materials on concrete resistance against carbonation and chloride ingress, Cem. Concr. Res. 30 (2000) 291–299.

[45] B. Johannesson, P. Utgenannt, Microstructural changes caused by carbonation of cement mortar, Cem. Concr. Res. 31 (2001) 925–931.

[46] A. Machner, M. Zajac, M. Ben, K.O. Kjellsen, M.R. Geiker, K. De Weerdt, Stability of the hydrate phase assemblage in Portland composite cements containing dolomite and

metakaolin after leaching , carbonation , and chloride exposure, Cem. Concr. Compos. 89 (2018) 89–106.

[47] L. Black, K. Garbev, I. Gee, Surface carbonation of synthetic C-S-H samples: A comparison between fresh and aged C-S-H using X-ray photoelectron spectroscopy, Cem. Concr. Res. (2008).

[48] L. Black, K. Garbev, G. Beuchle, P. Stemmermann, D. Schild, X-ray photoelectron spectroscopic investigation of nanocrystalline calcium silicate hydrates synthesised by reactive milling, Cem. Concr. Res. 36 (2006) 1023–1031.

[49] M. Thiery, G. Villain, P. Dangla, G. Platret, Investigation of the carbonation front shape on cementitious materials: Effects of the chemical kinetics, Cem. Concr. Res. 37 (2007) 1047–1058.

[50] Y. Xi, Z.P. Bazant, L. Molina, H.M. Jennings, Moisture diffusion in cementitious materials, Advn. Cem. Bas. Mat. 1 (1994) 258–266.

[51] Y. Houst, F.H. Wittmann, Diffusion de gaz et durabilité du béton armé, in: IABSE Symp. Durab. Struct., Lisbon, 1989: pp. 139–144.

[52] A.E. Morandeau, M. Thiery, P. Dangla, C.E. White, Accelerated carbonation modelling of fly ash-blended cement paste, in: RILEM Int. Symp. Concr. Model., Beijing, China, 2014.

[53] I.G. Richardson, The nature of C-S-H in hardened cements, Cem. Concr. Res. 29 (1999) 1131–1147.

[54] Q.T. Phung, N. Maes, E. Jacops, D. Jacques, G. De Schutter, G. Ye, Insights and issues on the correlation between diffusion and microstructure of saturated cement pastes, Cem. Concr. Compos. 96 (2018) 106–117.

[55] F. Lollini, E. Redaelli, L. Bertolini, Cement & Concrete Composites Effects of portland cement replacement with limestone on the properties of hardened concrete, Cem. Concr. Compos. 46 (2014) 32–40.

[56] R. Bucher, P. Diederich, G. Escadeillas, M. Cyr, Service life of metakaolin-based concrete exposed to carbonation: Comparison with blended cement containing fly ash, blast furnace slag and limestone filler, Cem. Concr. Res. 99 (2017) 18–29.